AD_____

GRANT NUMBER: DAMD17-94-J-4381

TITLE: Rapid 4D MRI of Gad-DTPA Enhancement for Breast Lesion Characterization

PRINCIPAL INVESTIGATOR: Thomas L. Chenevert, Ph.D.

CONTRACTING ORGANIZATION: University of Michigan
Ann Arbor, Michigan 48109-1274

REPORT DATE: October 1995

TYPE OF REPORT: Annual

PREPARED FOR: U.S. Army Medical Research and Materiel Command
Fort Detrick, Maryland 21702-5012

# REPORT DOCUMENTATION PAGE

*Form Approved*
*OMB No. 0704-0188*



| 1. AGENCY USE ONLY *(Leave blank)* | 2. REPORT DATE | 3. REPORT TYPE AND DATES COVERED |
|---|---|---|
| | October 1995 | Annual 1 Oct 94 - 30 Sep 95 |

**4. TITLE AND SUBTITLE**
Rapid 4D MRI of Gad-DTPA Enhancement for Breast Lesion Characterization

**5. FUNDING NUMBERS**
DAMD17-94-J-4381

**6. AUTHOR(S)**
Thomas L. Chenevert, Ph.D.

**7. PERFORMING ORGANIZATION NAME(S) AND ADDRESS(ES)**
University of Michigan
Ann Arbor, Michigan 48109-1274

**8. PERFORMING ORGANIZATION REPORT NUMBER**

**9. SPONSORING/MONITORING AGENCY NAME(S) AND ADDRESS(ES)**
U.S. Army Medical Research and Materiel Command
Fort Detrick, Maryland 21702-5012

**10. SPONSORING/MONITORING AGENCY REPORT NUMBER**

**11. SUPPLEMENTARY NOTES**

**12a. DISTRIBUTION/AVAILABILITY STATEMENT**
Approved for public release; distribution unlimited

**12b. DISTRIBUTION CODE**

**13. ABSTRACT** *(Maximum 200 words)*

The objectives of this project are refinement and clinical application of new methods designed to defeat the tradeoff between spatial resolution, temporal resolution and acquisition volume in dynamic gadolinium-enhanced MR mammography. The approach, referred to as "3D keyhole" involves specialized software for data acquisition and reconstruction that allow dynamic scans of 32 sections through both breasts to be acquired at 13second temporal resolution. This methodology provides greater precision in numerical fitting of temporal enhancement features of lesions. Extensive data processing tools have been developed to visualize dynamic contrast changes and reduce lesion temporal enhancement curves to fitted time and amplitude constants. This methodology is being applied in a prospective 4 year study of 100 women in whom a breast abnormality, detected by conventional means, is to be characterized by surgical biopsy. The targeted patient accrual in of 25 patients per year has been achieved. The hypothesized trend for malignancies to display rapid/strong contrast enhancement due to angiogenesis is apparent, although, some false positives and negatives do persist.

**14. SUBJECT TERMS**
breast neoplasm diagnosis
gadolinium-DTPA contrast agent
angiogenesis
breast cancer
dynamic magnetic resonance imaging
tumor vascularity
enhancement time-course analysis

**15. NUMBER OF PAGES**
16

**16. PRICE CODE**

| 17. SECURITY CLASSIFICATION OF REPORT | 18. SECURITY CLASSIFICATION OF THIS PAGE | 19. SECURITY CLASSIFICATION OF ABSTRACT | 20. LIMITATION OF ABSTRACT |
|---|---|---|---|
| Unclassified | Unclassified | Unclassified | Unlimited |

## GENERAL INSTRUCTIONS FOR COMPLETING SF 298

The Report Documentation Page (RDP) is used in announcing and cataloging reports. It is important that this information be consistent with the rest of the report, particularly the cover and title page. Instructions for filling in each block of the form follow. It is important to ***stay within the lines*** to meet ***optical scanning requirements***.

**Block 1.** Agency Use Only *(Leave blank)*.

**Block 2.** Report Date. Full publication date including day, month, and year, if available (e.g. 1 Jan 88). Must cite at least the year.

**Block 3.** Type of Report and Dates Covered. State whether report is interim, final, etc. If applicable, enter inclusive report dates (e.g. 10 Jun 87 - 30 Jun 88).

**Block 4.** Title and Subtitle. A title is taken from the part of the report that provides the most meaningful and complete information. When a report is prepared in more than one volume, repeat the primary title, add volume number, and include subtitle for the specific volume. On classified documents enter the title classification in parentheses.

**Block 5.** Funding Numbers. To include contract and grant numbers; may include program element number(s), project number(s), task number(s), and work unit number(s). Use the following labels:

| | | | |
|---|---|---|---|
| **C** | - Contract | **PR** | - Project |
| **G** | - Grant | **TA** | - Task |
| **PE** | - Program Element | **WU** | - Work Unit Accession No. |

**Block 6.** Author(s). Name(s) of person(s) responsible for writing the report, performing the research, or credited with the content of the report. If editor or compiler, this should follow the name(s).

**Block 7.** Performing Organization Name(s) and Address(es). Self-explanatory.

**Block 8.** Performing Organization Report Number. Enter the unique alphanumeric report number(s) assigned by the organization performing the report.

**Block 9.** Sponsoring/Monitoring Agency Name(s) and Address(es). Self-explanatory.

**Block 10.** Sponsoring/Monitoring Agency Report Number. *(If known)*

**Block 11.** Supplementary Notes. Enter information not included elsewhere such as: Prepared in cooperation with...; Trans. of...; To be published in.... When a report is revised, include a statement whether the new report supersedes or supplements the older report.

**Block 12a.** Distribution/Availability Statement. Denotes public availability or limitations. Cite any availability to the public. Enter additional limitations or special markings in all capitals (e.g. NOFORN, REL, ITAR).

**DOD** - See DoDD 5230.24, "Distribution Statements on Technical Documents."
**DOE** - See authorities.
**NASA** - See Handbook NHB 2200.2.
**NTIS** - Leave blank.

**Block 12b.** Distribution Code.

**DOD** - Leave blank.
**DOE** - Enter DOE distribution categories from the Standard Distribution for Unclassified Scientific and Technical Reports.
**NASA** - Leave blank.
**NTIS** - Leave blank.

**Block 13.** Abstract. Include a brief *(Maximum 200 words)* factual summary of the most significant information contained in the report.

**Block 14.** Subject Terms. Keywords or phrases identifying major subjects in the report.

**Block 15.** Number of Pages. Enter the total number of pages.

**Block 16.** Price Code. Enter appropriate price code *(NTIS only)*.

**Blocks 17. - 19.** Security Classifications. Self-explanatory. Enter U.S. Security Classification in accordance with U.S. Security Regulations (i.e., UNCLASSIFIED). If form contains classified information, stamp classification on the top and bottom of the page.

**Block 20.** Limitation of Abstract. This block must be completed to assign a limitation to the abstract. Enter either UL (unlimited) or SAR (same as report). An entry in this block is necessary if the abstract is to be limited. If blank, the abstract is assumed to be unlimited.

## FOREWORD

Opinions, interpretations, conclusions and recommendations are those of the author and are not necessarily endorsed by the US Army.

NA Where copyrighted material is quoted, permission has been obtained to use such material.

NA Where material from documents designated for limited distribution is quoted, permission has been obtained to use the material.

VC Citations of commercial organizations and trade names in this report do not constitute an official Department of Army endorsement or approval of the products or services of these organizations.

NA In conducting research using animals, the investigator(s) adhered to the "Guide for the Care and Use of Laboratory Animals," prepared by the Committee on Care and Use of Laboratory Animals of the Institute of Laboratory Resources, National Research Council (NIH Publication No. 86-23, Revised 1985).

VC For the protection of human subjects, the investigator(s) adhered to policies of applicable Federal Law 45 CFR 46.

NA In conducting research utilizing recombinant DNA technology, the investigator(s) adhered to current guidelines promulgated by the National Institutes of Health.

NA In the conduct of research utilizing recombinant DNA, the investigator(s) adhered to the NIH Guidelines for Research Involving Recombinant DNA Molecules.

NA In the conduct of research involving hazardous organisms, the investigator(s) adhered to the CDC-NIH Guide for Biosafety in Microbiological and Biomedical Laboratories.

Thomas J Conners 10/26/95

PI - Signature Date

**TABLE OF CONTENTS** **Page**

## INTRODUCTION

It is generally accepted that comparison of pre- versus post-gadolinium (gadopentetate dimeglumine) enhanced gradient recalled echo MRI offers exceptionally high sensitivity for the detection of breast cancers [1-6]. The specificity of gadolinium-enhanced MR mammography to distinguish benign from malignant tissues, however, has been limited by the fact that some normal and benign masses also exhibit contrast enhancement [3,5,6]. The "temporal rate" of gadolinium enhancement has also generated considerable interest as a potential complimentary discriminator of benign and malignant breast neoplasm [7-10]. The underlying mechanism of contrast enhancement rate as a diagnostic parameter relates to tissue vascularity which has been shown to be a key correlate in the growth and metastatic potential of breast malignancies. Non-invasive methods to detect and/or discriminate between normal, benign, pre-malignant and malignant tissues based on vascularity hold inherent diagnostic promise by virtue of this link to tumor angiogenesis.

Acquisition and processing methods to quantify enhancement rate, or temporal properties in general, have been widely variable across studies [7-10]. In the assessment of temporal enhancement features, critical parameters include temporal resolution, volume of tissue coverage, and the method to quantify signal evolution. Information regarding kinetics will be obscured if the temporal resolution is inadequate to sample rapid signal changes or enhancement curve shape details. Problems also arise if the dynamically imaged volume only partially includes an enhancing lesion or does not include all lesions in the breast. These issues arise, in part, because of the inevitable trade-off in standard MRI acquisition techniques between volume coverage, spatial resolution, and temporal resolution. Central to this project are refinement and clinical application of new methods designed to partially defeat this tradeoff in providing full volume coverage of both breasts at good spatial and temporal resolution for detailed quantification of dynamic contrast enhancement [10]. The approach, referred to as "3D keyhole" involves specialized software for data acquisition (i.e. MRI pulse sequence) and reconstruction. This methodology allows dynamic scans through 32 sections of both breasts to be acquired at 13second temporal resolution (compared to commonly used ≈minute resolution in volume scans). A major practical advantage of this technique is the ability to retrospectively select and analyze multiple arbitrary tissues/lesions within either breast that would otherwise not identified prior to contrast administration. Extensive data processing tools have been developed to visualize dynamic contrast changes and reduce temporal enhancement curves of lesions to numerically fitted time and amplitude constants. This methodology is being applied in a prospective study of 100 women in whom a breast abnormality, detected by conventional means, will be characterized by surgical biopsy.

## METHODS

*Technical*

Breast MR exams are performed on either of our two 1.5T General Electric Signa systems using a commercial bilateral phased-array breast coil with insert pads for mild A/P compression. After a quick locator scan, conventional axial T2-wt fast-spin-echo is performed to identify cysts. Axial pre- and post-gadolinium T1-wt spin-echo bracket the "dynamic scan" described below.

Dynamic scans consist of three segments all within one series prescription:

a) Pre-Gad Reference: A coronal 3D rf-spoiled gradient recalled echo (3D SPGR) is prescribed to encompass both breasts. Parameters are: TR=13ms; TE=4.5ms; flip=40°; NEX=4; typical FOV=30cm (R/L), 15cm (S/I), 3mm slice thk; matrix=256 (R/L), 128 (S/I), 32 slices (A/P); acquisition time=3'30". Raw time-domain data is automatically written to disk.

b) Dynamic-Gad: A flag is set for acquisition of central 256 ($k_{R/L}$) x 32 ($k_{S/I}$) x 32 ($k_{A/P}$) k-space (3D keyhole) data in 20 serial passes at 13seconds each pass (NEX=1). A full resolution matrix "21st pass" is automatically concatenated at the end for an acquisition time of 5'19". A 10sec bolus injection of 0.1mM/kg of gadolinium-DTPA (Magnevist) is administered with 4'45" remaining in the scan. Rawdata is automatically written to disk.

c) Post-Gad Scan: A flag is set to repeat scan with parameters in listen in a).

The total MR exam time is typically 40-45 minutes.

Raw data is networked to a SUN SPARC10 for offline 3D keyhole processing. This involves some corrections and insertion of each keyhole dataset into the full matrix reference dataset, then 3D Fourier transform to yield 32 slices at each of 20 timepoints. The 21st pass dataset is used to correct an enhancement amplitude error that results from partial k-space acquisition [10]. Keyhole reconstructed images and "reference-subtracted" images are viewed cinegraphically. Enhancing lesions are best perceived in this format which guides ROI definition. Lesion enhancement time-course curves are then automatically fit to mono- and double-exponential saturation models such that temporal features are reduced to enhancement time-constants [10]. Additional software has been written to cinegraphically display maximum-intensity-projection (MIP) of subtracted images through the full 3D volume and display heterogeneity of fitted constants within the defined ROI.

*Clinical*

Recruited patients are referred from the Breast Imaging Section of the Breast Care Center at the University of Michigan Hospital. Entrance criteria includes any patient with a breast abnormality detected by mammography, physical examination, or ultrasound which will be biopsied. Prior to MRI study, all patients have a routine clinical evaluation which includes, as a minimum, mammography and breast physical examination. Twenty-five patients were to be studied in each of 4years. Twenty-seven patients have been studied to date in Year1.

Three radiologists independently review the data from the following "modalities" in the order of: (a) conventional mammography images (Xray, ultrasound) and reports; (b) conventional MRI including pre- and post-gadolinium; and (c) subtracted MR images (pre-gad subtracted from post-gad). Readers grade lesions on five point scales of suspicion (benign to malignant) and visibility (obvious to subtle).

The temporal enhancement properties of tissues/masses are quantified by numerical fit to the 21 points of the enhancement curve to yield mono- and double-exponential saturation

time constants and enhancement amplitudes. Time-course data, fitted curves and related fit parameters are stored on disk as a permanent ROI record.

## RESULTS

Determination of the diagnostic power of temporal contrast enhancement properties as quantified by time-constants is central to the goal of this research. We have combined data from Year 1 (27 patients) to that of our pilot study using similar methodology to increase the study population to 41 patients. A scatterplot of fitted mono-exponential time constant versus tissue type is illustrated in the figure.

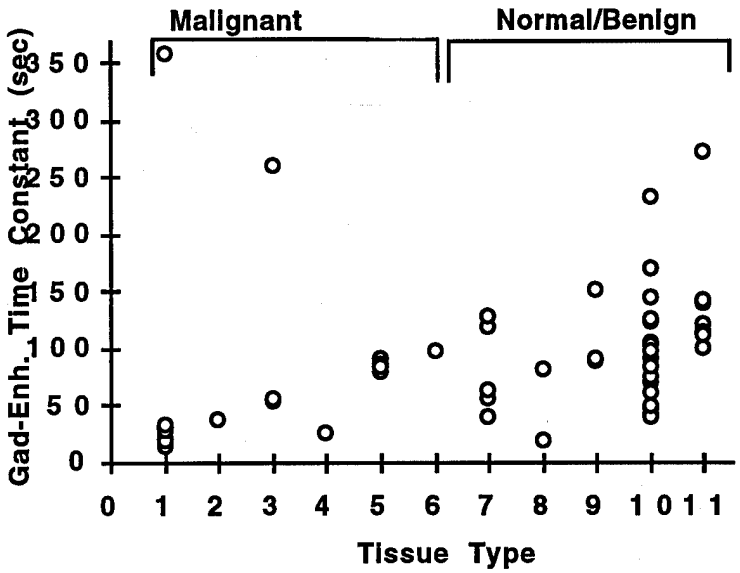


Tissue Type Key:

1 = Inv Ductal Ca
2 = Neuroendocrine Ca
3 = Inv Lobular Ca
4 = IntraDuctal Ca
5 = Adj. to InvDuctal Ca
6 = Lobular Ca InSitu
7 = Fibroadenoma
8 = Fibrocystic change
9 = Benign mass
10 = Nipple / Areola
11 = Normal parenchyma

Figure: Enhancement time constant vs tissue type

## CONCLUSIONS

Study hypotheses relate to the diagnostic value of contrast enhancement temporal features in distinguishing benign from malignant and between tissue/tumor types. The hypotheses for testing state that a high rate of contrast change (i.e. short enhancement time constant) raises suspicion of malignancy. While the data generated thus far are limited by patient numbers, the trend for malignancies to exhibit rapid enhancement relative to non-malignant tissues is apparent. Diagnosis based solely on enhancement temporal features, however, does not guarantee against false positives or, more seriously, false negatives as indicated in the figure. The prevalence of these misclassifications require greater patient volume as planned for the remainder of the study.

## REFERENCES


1. Heywang SH, Hahn D, Schmidt H, et al. MR imaging of the breast using gadolinium-DTPA. J Comput Assist Tomogr 1986; 10(2):199-204.
2. Heywang SH, Wolf A, Pruss E, Hilbertz T, Eiermann W, Permanetter W. MR imaging of the breast with Gd-DTPA: use and limitations. Radiology 1989; 171(1):95-103.
3. Pierce WB, Harms SE, Flamig DP, Griffey RH, Evans WP, Hagans JE. Three-dimensional gadolinium-enhanced MR imaging of the breast: pulse sequence with fat suppression and magnetization transfer contrast. Work in progress. Radiology 1991; 181(3):757-763.
4. Harms SE, Flamig DP, Hesley KL, et al. MR imaging of the breast with rotating delivery of excitation off resonance: clinical experience with pathologic correlation. Radiology 1993; 187(2):493-501.
5. Harms SE, Flamig DP. MR imaging of the breast: technical approach and clinical experience. Radiographics 1993; 13(4):905-912.
6. Heywang-Kobrunner SH. Contrast-enhanced magnetic resonance imaging of the breast. Invest Radiol 1994; 29(1):94-104.
7. Kaiser WA, Zeitler E. MR imaging of the breast: fast imaging sequences with and without Gd- DTPA. Preliminary observations. Radiology 1989; 170(3 Pt 1):681-686.
8. Stack JP, Redmond OM, Codd MB, Dervan PA, Ennis JT. Breast disease: tissue characterization with Gd-DTPA enhancement profiles. Radiology 1990; 174(2):491-494.
9. Orel SG, Schnall MD, Li Volsi VA, Troupin RH. Suspicious breast lesions: MR imaging with radiologic-pathologic correlation. Radiology 1994; 190(2):485-493.
10. Chenevert TL, Helvie MA, Aisen AM, et al. Dynamic three-dimensional imaging with partial K-space sampling: initial application for gadolinium enhanced rate characterization of breast lesions. Radiology 1995; 196:135-142.


## APPENDIX

Reprint of:

"Dynamic Three-dimensional Imaging with Partial K-Space Sampling: Initial Application for Gadolinium-enhanced Rate Characterization of Breast Lesions";
Radiology 1995; 196: 135-142

Thomas L. Chenevert, PhD • Mark A. Helvie, MD • Alex M. Aisen, MD • Isaac R. Francis, MD
Dorit D. Adler, MD • Marilyn A. Roubidoux, MD • Frank J. Londy, RTR

# Dynamic Three-dimensional Imaging with Partial K-Space Sampling: Initial Application for Gadolinium-enhanced Rate Characterization of Breast Lesions[1]

*PURPOSE:* **To evaluate a method to monitor gadolinium enhancement patterns at magnetic resonance (MR) imaging with high temporal resolution and full coverage through both breasts.**

*MATERIALS AND METHODS:* **In 12 patients with 13 masses, including nine carcinoma, nonenhanced three-dimensional MR imaging was performed with full-matrix resolution. At dynamic imaging, 32 serial passes were made during bolus administration of contrast material, and temporal resolution was reduced to 12 seconds by collecting the central (low spatial frequency) 32 × 16 or 16 × 16 phase-encode views. Full-matrix dynamic images were reconstructed by complementing central phase-encode data with precontrast data from peripheral high-spatial-frequency views.**

*RESULTS:* **Results at time-course analysis with a mono-exponential saturation model indicated malignant lesions tend to show rapid (<60 seconds) contrast change relative to benign masses and normal tissues. One cancer displayed an exceptionally slow contrast change (260 seconds).**

*CONCLUSION:* **The technical objectives of full tissue coverage, rapid temporal sampling, and quantification of enhancement curves are met with this method for certain lesions (>5 mm in largest diameter).**

**Index terms:** Breast, MR, 00.12143 • Breast neoplasms, MR, 00.12143 • Magnetic resonance (MR), k-space

**Radiology 1995;** 196:135–142

EARLY magnetic resonance (MR) imaging demonstrated only limited success in assisting diagnosis of breast disease (1–4). Initially, only tissue-inherent differences in nuclear MR relaxation times, T1 and T2, were the primary sources of contrast. Although these contrasts are relatively high, it was observed that they have little value in helping detection and diagnosis of breast cancer (1,3,5,6). Variable admixtures of intense fat signal and inadequate fat suppression have also seriously hindered image interpretation and detection of breast carcinoma.

More recently, gadolinium-enhanced MR mammography has generated considerable interest (7–10). It is generally accepted that gadolinium enhanced MR imaging offers high sensitivity for the detection of breast cancers. The specificity of gadolinium-enhanced MR mammography to distinguish benign from malignant tissues, however, has been limited by the fact that benign tissues can also exhibit contrast enhancement (9,11,12).

The rate of gadolinium enhancement has also been studied as a potential discriminator of benign and malignant breast neoplasms (13–15). In their initial summary of findings in 25 patients who underwent dynamic gadolinium-enhanced MR imaging, Kaiser and Zeitler reported that all malignancies displayed rapid enhancement (ie, ~100% increase in signal intensity within the first 2 minutes after injection of 0.1 mmol/kg gadopentetate dimeglumine), whereas benign lesions demonstrated less and slower signal intensity change (13). These authors have since updated their dynamic gadolinium-enhanced MR imaging study, in which sensitivity and specificity for cancer detection was greater than 95% (16). In other dynamic gadolinium-enhanced MR imaging studies, higher false-positive rates were observed; thus, there is not a consensus among investigators on methods or diagnostic value of this approach (11,12,17). Findings in these and other studies illustrate that fibroadenomas and proliferative fibrocystic change, in particular, are sources of false-positive findings. Breast malignancies typically exhibit rapid enhancement while benign lesions usually, although not necessarily, exhibit slower contrast change. Malignant lesions may enhance slowly, thus reducing sensitivity (12,18).

Use of various acquisition and enhancement rate quantification schemes may contribute to discrepancies in findings (13–15). In assessment of enhancement rate, important parameters include temporal resolution, volume of tissue covered, and the method used to quantify signal intensity change. In particular, important information on the rate of enhancement may be obscured if the temporal resolution is inadequate to sample rapid contrast changes. In addition, problems will obviously arise if the dynamic imaging volume includes an enhancing lesion only partially or does not include all lesions in the breast. These issues arise in part because there is an inevitable trade-off in standard MR imaging between imaged volume and temporal resolution.

MR imaging with methods such as high spatial resolution, three-dimensional (3D) volumes, suppression of fat signal, and magnetization transfer contrast have been studied in an at-

[1] From the Department of Radiology, University of Michigan Medical Center, 1500 E Medical Center Dr, Ann Arbor, MI 481090030 (T.L.C., M.A.H., I.R.F., D.D.A., M.A.R., F.J.L.); and the Department of Radiology, Indiana University Hospital, Indianapolis (A.M.A.). Received July 28, 1994; revision requested September 14; revision received January 31, 1995; accepted February 6. Supported in part by the National Institutes of Health grant lP30 CA46592, a research award from the Society of Computed Body Tomography and Magnetic Resonance, and U.S. Army grant DAMD17-94-J-4381. **Address reprint requests to** T.L.C.


**Abbreviations:** ROI = region of interest, 3D = three-dimensional.

tempt to produce high-quality anatomic images (9,19). These 3D acquisitions typically require several minutes; thus, dynamic properties are not readily observed. Conversely, to improve temporal sampling of enhancement curves, others have performed two-dimensional multisection MR imaging with 1-minute temporal resolution (13) or of one judiciously selected section with finer temporal (15-second) resolution (14). Unfortunately, selection of prospective section(s) for dynamic MR imaging by means of correlation with findings at x-ray mammography, ultrasonography (US), or physical examination can be extremely difficult in the amorphous anatomy of a variably compressed breast, except in cases of large tumors. Moreover, the nonspecific features of some lesions on precontrast MR images may further hinder prospective selection of appropriate section(s) for dynamic imaging.

The central objective of this study was to obviate the trade-off between tissue coverage and temporal resolution seen in other studies of dynamic gadolinium-enhanced MR imaging of the breast. The specific technical objectives were development and validation of a pulse sequence that would *(a)* monitor gadolinium enhancement on a short time scale ($\approx$ 12 seconds), *(b)* image the full volume of both breasts, *(c)* produce anatomic images with sufficient spatial resolution and contrast to allow correlation of findings with those on images obtained with other modalities, and *(d)* quantify parameters related to enhancement rate.

## MATERIALS AND METHODS

### Patients

Twelve female patients, aged 30–62 years (mean, 48 years), were recruited for this study. Eleven patients had one or multiple masses identified at mammography and/or physical examination. Pathologic confirmation was obtained in 11 of 13 masses, including nine invasive carcinoma tumors (largest diameter mean, 22 mm; range, 12–50 mm) in seven patients and in the one benign mass in each of two patients (fibrosis with largest diameter of 30 mm and a palpable benign mass with largest diameter of 10 mm). Of the remaining two of 13 masses, one was a palpable mass with a largest diameter of 20 mm that resolved with time in one patient and was therefore presumed to be benign and the other was a mass with a largest diameter of 17 mm that was radiographically consistent with a fibroadenoma and was stable for 7 years in another patient. Cytologic findings were also consistent with a fibroadenoma. One patient had no detectable mass and was presumed to have no breast disease. The MR imaging methods were approved by an institutional review board, and informed written consent was obtained from all participants.

### Data Acquisition for 3D Keyhole MR Imaging

Patients underwent imaging on a Signa imager (GE Medical Systems, Milwaukee, Wis). Plane orientation and field of view for the dynamic series were chosen to allow efficient imaging of the breasts with high spatial resolution and minimal image wraparound and involvement of the heart. Coronal imaging was performed through the suspended breasts with use of a rectangular field of view with matrix dimensions of 256 (right to left) × 128 (superior to inferior) pixels as the preferred geometry. In eight patients imaging was performed with a dedicated breast coil. In four other patients imaging was performed with the patient lying prone on a surface coil, as a result of body habitus, and axial dynamic imaging was necessary in two of these patients. The remainder of the dynamic studies were performed with coronal views.

The patients initially underwent localization with conventional nonenhanced T1- and T2-weighted, spin-echo sequences. Conventional enhanced spin-echo, T1-weighted imaging was also performed. A reduced k space or "keyhole" technique (20–22), described in detail below, was used for dynamic imaging. Precontrast acquisitions, referred to as reference data sets, were performed with a 3D matrix of 256 × 128 × 32 sections and one signal acquired.

Reference imaging was followed immediately with dynamic 3D keyhole imaging, without changing the hardware settings, and only the central phase-encode views (in both phase-encode directions) were serially imaged in 32 passes during administration of contrast material. In nine of the 12 patients studied, 3D keyhole dimensions were 256 × 32 × 16 (ie, one-eighth of k space acquired), and in the remaining three patients 3D keyhole dimensions were 256 × 16 × 16 (ie, one-sixteenth of k space acquired). Timing parameters included repetition time of 24 msec and echo time of 4.5 msec (24/4.5) for the 256 × 32 × 16 keyhole acquisitions and 45/7 for the 256 × 16 × 16 keyhole acquisitions. Temporal resolution, defined as the time to complete each keyhole pass, was comparable in all acquisitions (ie, 12.3 and 11.5 seconds, respectively). Reference and dynamic keyhole imaging were both performed with use of the same radio-frequency-spoiled sequence of gradient-recalled acquisition in the steady state, which included a frequency-selective, fat-saturation pulse. Other imaging parameters included a 40° flip angle, one signal acquired, 32-bit digitization, and ±32-kHz bandwidth. The nominal right-to-left field of view of 300 mm and section thickness of 3–6 mm (mean, 4.5 mm) were adjusted for patient size. The position and thickness of 3D slabs (equal to 28 sections) were graphically prescribed on orthogonal images to encompass the volume of the breasts. Imaging times for reference and serial 3D keyhole acquisitions, respectively, were 1 minute 39 seconds and 6 minutes 33 seconds with repetition time of 24 msec, and 3 minutes 5 seconds and 6 minutes 9 seconds with repetition time of 4 msec.

In all cases, 0.1 mmol/kg of gadopentetate dimeglumine (Magnevist; Berlex Laboratories, Wayne, NJ) was manually injected as a bolus over 10–15 seconds in an antecubital vein. The injection was started 5 minutes 30 seconds before the end of dynamic imaging. After dynamic imaging, the raw data were permanently stored (requiring 1–2 minutes). Then a full-matrix series was obtained with the same imaging parameters used for the reference data set to enable comparison of pre- and postcontrast images.

### Data Processing

Time-domain data from precontrast and dynamic acquisitions were transferred to a computer (Sparc10; Sun Microsystems, Mountain View, Calif) for off-line processing. Custom software tools for reconstruction, display, and region-of-interest (ROI) analysis were written for processing (Advanced Visual Systems, Waltham, Mass). Modules were also written to determine phase differences between the early dynamic passes (ie, prior to changes in contrast) and the corresponding central time-domain data of the full-matrix reference data set. Ideally, these should have identical phase. Slight patient repositioning, however, could result in phase error and artifact on reconstructed keyhole images. Therefore, phase differences were determined and, when necessary, a single phase-correction setting was applied to all 32 temporal passes of each study.

After phase correction, each pass was substituted for the central-time-domain core of the full-matrix reference data set and was reconstructed into a 32-section image set by means of conventional 3D Fourier transform. This process was repeated for all passes to produce 1,024 anatomic images (32 sections × 32 time points). Subtraction images were also produced by using an early time point as a mask. Anatomic and subtraction images versus time were viewed side by side cinegraphically. Other display formats designed for quick survey of data sets included an image matrix of all sections (anatomic and subtracted images) at the last time point and cinegraphic display of maximum intensity projections of subtracted images. The maximum-intensity-projection images were obtained through the full tissue volume along orthogonal views and were particularly beneficial for viewing changes in spatial and temporal contrast of the lesion(s) relative to the heart and large vessels.

The time course of signal change in an ROI of enhancing tissues was fit to a mono-exponential saturation model with use of a Levenberg-Marquardt least-squares optimization algorithm (23). Fitted parameters include contrast onset, $t_o$; amplitude of signal change, $A$; and enhancement time constant, $\tau$, used within the following model:

$$\Delta S(t) = \begin{cases} A[1 - e^{-(t-t_0)/\tau}], \text{ for } t > t_0 \\ 0, \text{ for } t \leq t_0. \end{cases} \quad (1)$$

## RESULTS

Regarding mass conspicuity, conventional precontrast spin-echo T1- and T2-weighted images frequently did not delineate location or spatial extent of the masses. Visual comparison of pre- versus postcontrast images (Tl-weighted spin-echo and gradient-recalled-echo images) was adequate to identify nearly all (12 of 13) palpable and/or mammographically detected masses. Mass detection and localization were facilitated by inspection of anatomic and subtracted cinegraphic images generated by means of the keyhole scheme. Subtraction removed many image features that partially obscured lesions, and cinegraphic display further delineated lesions in terms of time and intensity of contrast change. As the cinegraphic format provided the greatest conspicuity of enhancing tissues, it was used to interactively guide ROI definition on the time-series images. One superficial palpable mass ($\approx$1 cm in largest diameter) displayed signal intensity enhancement, although the enhancement was not distinct relative to surrounding tissues. The mass region was identified as a capsule on the skin that was visible at MR imaging. This mass was occult at conventional x-ray mammography and US and was shown to be benign at pathologic analysis.

Figure 1 illustrates data obtained in a 56-year-old patient with pathologically proved invasive lobular carcinoma in two adjacent sites separated by approximately 1 cm. Mammograms depicted only the larger mass. An early-time-point (ie, before contrast intensity change) keyhole image (Fig 1a) does not depict the two malignant foci, which were most apparent on the late-time-point subtraction keyhole image (Fig 1b). Keyhole matrix size applied in this case was 256 × 32 × 16. Several keyhole subtraction images from the 32-image time series for this section are shown in Figure 1c. While the relatively rapid enhancement period is visually apparent in the time series, temporal contrast patterns of various tissues are best viewed graphically, as shown in Figure 1d. Mono-exponential parameters and fitted curves are also shown in this plot. The time constants of the lesions ($\tau$ = 52 or 55 seconds) indicate that the majority of signal intensity change occurs in less than 1 minute. The number or location of these masses was not readily apparent on precontrast images (Fig 1a), although their region roughly correlated with a suspect mass seen on the mammogram.

An example of a slowly enhancing lesion is Figure 2, which was obtained in a 56-year-old patient with a probable fibroadenoma. Findings at MR imaging and mammography were easily correlated for this particular mass, which had been sampled cytologically 7 years earlier. No change in size was seen, as noted in Materials and Methods. A subset of the subtraction-image time series illustrates gradual enhancement of the lesion (Fig 2c). The keyhole matrix size applied in this case was also 256 × 32 × 16. As with the data in Figure 1d, the time-course curve is well fit by an exponential (Fig 2d), although for this lesion the time constant is substantially longer ($\tau$ = 119 seconds).

A summary of fitted mono-exponential time constants for a variety of tissue types and all patients is shown in the scatter plot of Figure 3. ROIs from tissues labeled "normal" were derived from areas remote to the mass that displayed sufficient enhancement for curve fitting but were otherwise normal in appearance. These were typically regions of diffuse enhancement from either the ipsilateral or contralateral breast. No more than one normal-tissue ROI was derived in each patient. Two of the five invasive ductal carcinoma tumors were found in one patient (within one breast and separated by approximately 5 cm), and two of the three invasive lobular carcinoma tumors were found in one patient (Fig 1). ROIs of tissues adjacent to invasive ductal carcinoma tumors were defined to avoid signal blur from the lesion focus. As mentioned in Materials and Methods, the keyhole matrix size was 256 × 16 × 16 in three of 12 patients. Masses characterized in these patients were three invasive ductal carcinoma tumors (with largest diameters of 18, 13, and 22 mm and $\tau$ of 14, 20, and 18 seconds, respectively) and one neuroendocrine carcinoma (largest diameter, 14 mm; $\tau$, 37 seconds).

There was a clear tendency for the malignant lesions to display rapid contrast changes ($\tau$ < 60 seconds) relative to benign or normal tissues. However, one invasive lobular cancer displayed an exceptionally long time constant with $\tau$ of 260 seconds. Pathologic examination revealed the tumor had a largest diameter of at least 1 cm (margin was positive at initial biopsy), gross size of 1.2 × 1.0 × 0.8 cm, no angiolymphatic invasion, and no extensive ductal carcinoma in situ; in addition, 17 of 17 lymph nodes were negative for malignancy.

## DISCUSSION

We tested a technique with which to perform dynamic, contrast material–enhanced MR imaging of the entire volume of both breasts with a temporal resolution of approximately 12 seconds. The usefulness of the method was explored in our study of 12 patients with a total of 13 breast masses. As found in other studies, we noted a trend for malignant cancers to display rapid enhancement relative to benign and normal tissues, although the presence of one slowly enhancing cancer was observed. This would be considered a false-negative case if the enhancement time constant were used as the sole diagnostic indicator of malignancy. The small number of patients in this study, however, prevents us from drawing statistically meaningful inferences regarding the diagnostic value of this technique. Technical issues aside, other investigators have noted both false-negative and false-positive findings relative to enhancement rate (11,12,17,18).

The viability of this approach for management of breast disease necessitates determination of sensitivity and specificity rates for each application. The role that we are currently evaluating is the contribution of incremental information beyond that provided with conventional imaging modalities when a suspect mass is detected. In this capacity, emphasis is placed on characterization of previously detected masses that are usually more than 5 mm in largest diameter. Lesion localization for eventual dynamic gadolinium-enhanced MR imaging is hindered by nonspecific lesion properties in precontrast MR images and/or by poor correlation of findings with those of other imaging modalities, owing to variable breast geometries and views. This problem is essentially solved with the 3D keyhole approach, which has the inherent features of complete coverage through both breasts and high temporal sampling of dynamic contrast

a.

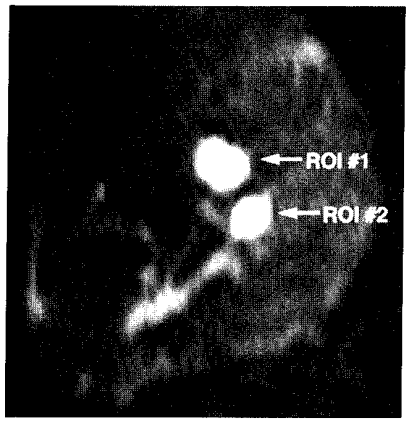


b.

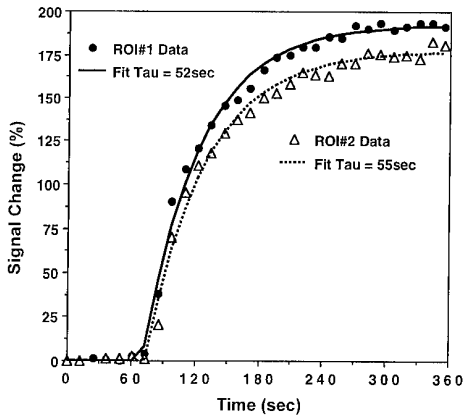


d.

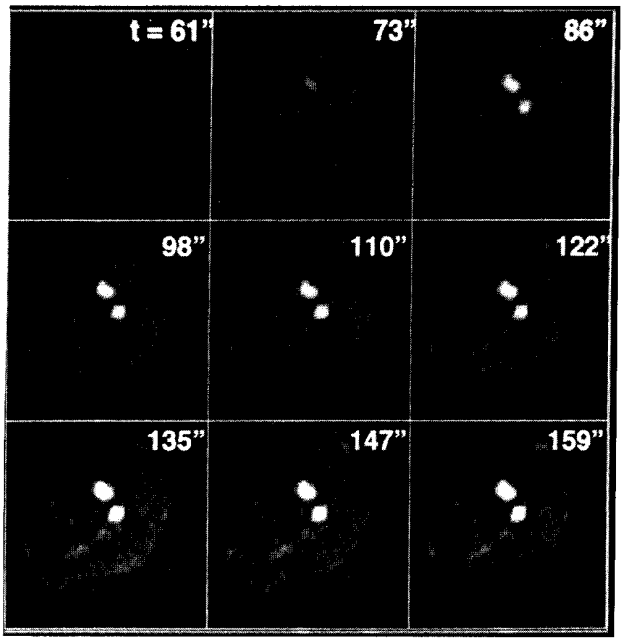


c.

**Figure 1.** Data from a coronal image obtained through the breast of a 56-year-old patient with two foci of invasive lobular carcinoma. **(a)** Early-time-point (ie, precontrast) keyhole image does not delineate the cancer tumors. **(b)** Subtraction image from a late time point ($\tau$ = 355 seconds) in dynamic imaging shows the two high-contrast cancer tumors (*ROI#1, ROI#2*). **(c)** Subset of time series for this section illustrates the relatively rapid contrast change in the cancer lesions. " = seconds. **(d)** Time-course analysis of regions *ROI#1* and *ROI#2* with use of mono-exponential saturation model whereby both cancers are characterized by a relatively short time constant ($\tau$ = 52, 55 seconds) (ie, a rapid contrast change). Images were electronically cropped to show only the area of interest.

changes. These advantages would also be a benefit in other potential applications, including use as an alternative breast screening modality in problematic cases (eg, dense breasts), as a survey modality to search for additional malignancies prior to lumpectomy, as an anatomic guide to direct biopsies, and potentially as an imaging modality in patients with serologic or genetic positive markers and negative findings at mammography. Our encouraging preliminary results suggest that further investigation with this technique is warranted.

The raw-data domain of MR imaging, referred to as k space, defines the spatial frequency distribution of an object and is a convenient format with which to describe various data acquisition schemes. In a simplistic sense, gross contrast features are primarily determined by data near the so-called center of k space (ie, low spatial frequencies), whereas features with high spatial detail are defined by data from more peripheral k space. These concepts are used with great success in techniques that generate desirable contrast properties more efficiently than routine MR imaging does (24,25).

Since most changes in object and temporal contrast are centralized in k space, other investigators have increased temporal resolution in dynamic gadolinium-enhanced two-dimensional keyhole MR imaging by repeatedly sampling only the central phase-encoded, $k_y$, lines (20). Images with high anatomic quality and temporal resolution are produced by combining dynamic data with previously acquired peripheral phase-encoded data. In application to the breast, a 3D acquisition is highly desirable for its advantages in tissue coverage, spatial resolution, and signal-to-noise ratio. The second phase-encode dimension, $k_z$, has an image-time penalty proportional to the number of sections. Fortunately, the keyhole concept may also be extended to this dimension so rapid dynamic volume imaging is possible (21, 22). One version of this sequence dynamically acquired only one-sixteenth of k space and was applied in three of 12 patients in this series; for the remaining studies, one-fourth of $k_y$ and one-half of $k_z$ (ie, one-eighth of k space) were dynamically acquired in one-eighth the image time.

The main drawback to sampling only a portion of k space is reduced spatial resolution. This is mitigated because dynamically acquired keyhole data can be complemented with previously acquired full-matrix data to generate high-resolution anatomic images. We emphasize, however, that temporally changing features remain blurred by an amount dependent on keyhole matrix size and lesion spatial dimensions. That is, spatial resolution in contrast-enhancing structures will be limited by the keyhole resolution and not by the full-matrix resolution. The rationale for splicing keyhole data into full-matrix reference data is that it provides the opportunity to view enhancing structures within a high-spatial-resolution format. In this format, morphologic cues such as stellate patterns or irregular borders of tissues or lesions are correctly associated with their dynamic enhance-

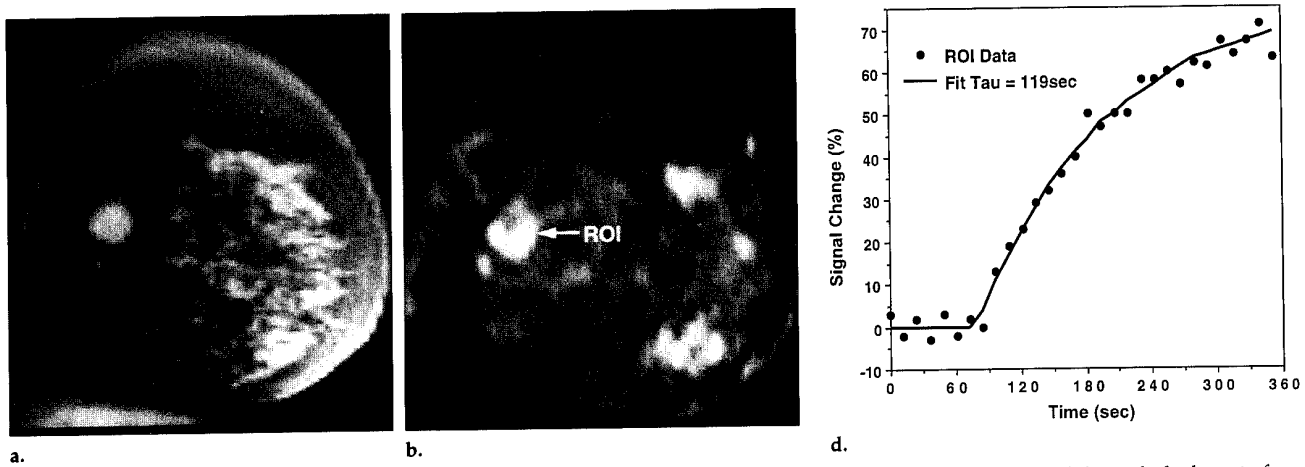


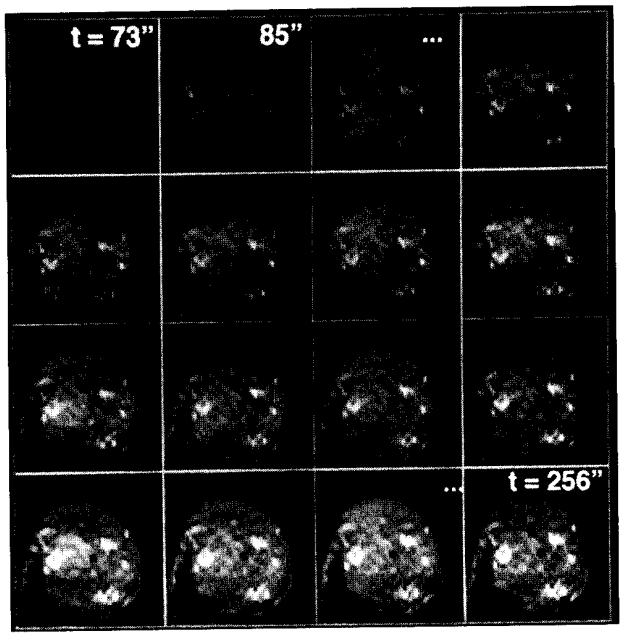


**Figure 2.** Data from a coronal image obtained through the breast of 56-year-old patient with a stable fibroadenoma. **(a)** Early-time-point (ie, precontrast) keyhole image. **(b)** Subtraction image from a late time point ($\tau$ = 355 seconds) of dynamic imaging shows contrast enhancement in the mass *(ROI)*. **(c)** Subset of time series for this section illustrates a gradual contrast change. " = seconds. **(d)** Time-course analysis of the mass indicates that this fibroadenoma has a moderate to long time constant ($\tau$ = 119 seconds).

ment properties. An alternative to the keyhole method is rapid acquisition of low-spatial-resolution data sets that are reconstructed and viewed independently from high-resolution data sets. However, we believe the complexities of keyhole reconstruction are justified to ensure the temporal enhancement profiles and spatial properties of a region are correctly related. Spatial blur of enhancement that results from acquisition of limited k space will spread along phase-encode directions to bordering tissue. That is, truly unenhancing tissues can demonstrate apparent enhancement that is actually caused by bleeding of signal intensity from adjacent enhancing tissues. Vertical smearing of signal intensity from small enhancing objects is illustrated in the subtraction images of Figures 1b and 2b.

In addition, the apparent amplitude of enhancement within truly enhanced tissue will be diminished. This effect in the phase-encode dimensions, y and z, is demonstrated with the function that characterizes a uniformly enhancing lesion as

$$\begin{aligned} L(y,z,t) &= L(y,z,0)\cdot[1 + C(t)] \\ &= \mathcal{FT}^{-1}\{L(k_y,k_z,0) \\ &\quad \cdot [1 + C(t)]\}, \end{aligned} \tag{2}$$

where $C(t)$ defines the temporal properties with $C(0)$ of 0 and $L(k_y,k_z,0)$ describes spatial properties of lesions in k space. Changes in contrast in the reconstructed keyhole image of this lesion, $\mathcal{L}(y,z,t)$, are limited by the spatial frequencies that lie within the sampled keyhole matrix. Thus for $K(k_y,k_z) \equiv 1$ within the keyhole range and zero otherwise, we have

$$\begin{aligned} \mathcal{L}(y,z,t) &= \mathcal{FT}^{-1}\{L(k_y,k_z,0) \\ &\quad \cdot [1 + K(k_y,k_z)\cdot C(t)]\}. \end{aligned} \tag{3}$$

The apparent enhancement time course of the lesion is derived by multiplying $\mathcal{L}(y,z,t)$ by an ROI mask and then performing spatial integration. The convolution theorem allows us to relate this in k space as

$$\begin{aligned} \Delta ROI(t) &= ROI(t) - ROI(0) \\ &= C(t)\int R(k_y,k_z) \\ &\quad \cdot L(k_y,k_z) \\ &\quad \cdot K(k_y,k_z)dk_y dk_z, \end{aligned} \tag{4}$$

where $R(k_y,k_z)$ is the Fourier transform of the ROI mask. If we assume the spatial pattern of the ROI closely matches that of the enhancing lesion, then $R(k_y,k_z) \approx L(k_y,k_z)$; thus, the integrand becomes $|L(k_y,k_z)|^2$ within the keyhole area and zero elsewhere. Finally, the full matrix acquisition is used to normalize the contrast suppression effect:

$$\Delta ROI(t) \cong \beta \cdot C(t) \cdot ROI(0);$$

where

$$\begin{aligned} \beta &= \left[\int_{\text{Keyhole area}} |L(k_y,k_z)|^2 dk_y dk_z\right] \\ &\quad \div \left[\int_{\text{Full K space}} |L(k_y,k_z)|^2 dk_y dk_z\right]. \end{aligned} \tag{5}$$

The factor $\beta$ represents the degree of suppression in contrast change that results from sampling only a portion of k space. For the above derivation to apply, the time to complete each keyhole pass must be short or must be at least comparable to the period of strong contrast change. The lesion contrast state is considered nearly constant for each keyhole pass but is allowed to vary from pass to pass. While coverage of full k space may

result in undersampling of temporal changes, such coverage is still used for normalization to provide a worst-case bound for β. Within the validity of these approximations, sampling of partial k space reduces the amplitude of the enhancement curve, although the temporal shape of the curve is correct. As a result, time-constant fitting of the shape of the enhancement curve is relatively immune to the effects of partial sampling of k space as long as the sampling period is adequately short and the signal-to-noise ratio is sufficiently high to enable detection of attenuated changes in signal.

For illustration, consider our default settings, in which one-eighth of k space is acquired with the 32 $k_y$ × 16 $k_z$ keyhole matrix. 3D acquisition with a rectangular 30 × 15-cm field of view and 4-mm sections gives phase-encode dimensions of 1.17 × 4.00-mm pixels. The change in suppression of signal intensity for a single-pixel (1.17 × 4.00 mm) lesion would be $\beta = 0.13$. That is, if a single-pixel lesion truly changed contrast by 100% (ie, the precontrast level doubled), results with this method would indicate only a 13% change in signal intensity. For larger lesions, the attenuation effect is lessened as the function $|L(k_y,k_z)|^2$ becomes peaked within the keyhole area.

Examples of predictions with Equation (5) in larger lesions obtained with the same acquisition parameters are $\beta = 0.46$ for a 4.70 × 4.00-mm lesion, $\beta = 0.81$ for a 8.20 × 8.0-mm lesion, and $\beta = 0.92$ for a 11.70 × 12.00-mm lesion. Composite cinegraphic display of anatomic and subtracted images partially overcomes the impact of contrast suppression. Subtraction removes time-invariant image features that partially obscure lesions, and cinegraphic display aids the observer in distinguishing true contrast changes from noise and other artifact.

Data obtained in large lesions in which $\beta \approx 1$ indicate signal intensity can be enhanced several times more than that depicted on nonenhanced images, but lesions with less change in signal intensity are also detectable and well quantified with enhancement-time constants. Assuming true changes in contrast are double the precontrast levels, we anticipate lesions more than 5 mm in diameter (where $\beta \approx 0.5$) would be detectable with this method since the apparent enhancement would be ≈50% or more. Of course, weaker enhancement or increased background noise or artifact would decrease conspicuity of these smaller lesions.

The high sensitivity of contrast-enhanced MR imaging for detection of breast disease is well known. Unfortunately, the modality has moderate specificity and is susceptible to false-positive findings, since some benign tumors and tissues also exhibit enhancement. Moreover if greater attention is to be paid to rapidly enhancing regions, normal structures need to be appropriately identified that naturally exhibit rapid signal change. Cinegraphic images viewed as individual sections (when acquired as such) or drawn from a 3D volume set display numerous small rapidly enhancing regions representing blood vessels. To help identification of vessels that can be potentially mistaken for small lesions, we further exploit the 3D nature of the data and produce maximum-intensity-projection images of subtraction images obtained through the full imaged volume along orthogonal directions. Section-to-section continuity of vessels is more easily appreciated in this display. These subtraction maximum-intensity-projection images are viewed cinegraphically, thus they also provide a quick survey of the full study. In this format, changes in spatial and temporal contrast of a mass relative to other breast tissues, vessels, and blood in the heart (usually partially included in the imaged volume) are readily apparent. Excerpts of a time series of superior-to-inferior maximum-intensity-projection images of subtraction images are shown in Figure 4a with enhancement-time-course curves for regions shown graphically in Figure 4b.

There are known fundamental tissue changes that provide the rationale for the hypothesis that malignant breast cancers will preferentially display rapid changes in contrast over most benign and normal tissues. Considerable experimental data show that tumors require an enhanced blood supply to support their rapid growth (26–28). Thermal diffusion–based delivery of nutrients sustains tumor nodules up to 1–2 mm in largest diameter, but their continued linear and rapid exponential growth to larger diameters is facilitated by neovascularity. Experimental evidence that tumors are angiogenesis dependent is summarized in an article by Folkman (29), in which several studies are cited that demonstrate tumor size is linear, slow, or stagnant before vascularization but switches to rapid growth after vascularization. Angiogenesis does not necessarily imply malignancy, however, since some benign tumors are also angiogenic. Significant correlations between tumor angiogenesis and invasiveness and metastatic potential of breast cancer have been demonstrated with direct optical microvessel counts in breast tumor specimens (26–28). There is also some evidence that precancerous breast tissues have a greater angiogenic propensity, suggesting that angiogenesis has potential as a precancer marker (30). Factors that trigger and moderate angiogenesis are not fully known, but their determination and potential exploitation for diagnosis and treatment are clearly critical areas for investigation.

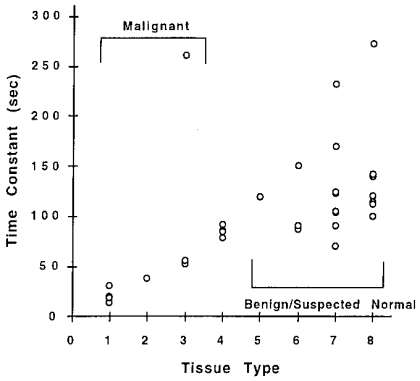


**Figure 3.** Scatter plot of time constants derived from time-course data for mono-exponential fits of enhancement. ROIs were defined on various tissue across 12 patients. The *N* values in the tissue type axis refer to the number of ROIs associated with each tissue type; only one ROI was defined for each discrete mass. One patient had two invasive ductal carcinoma tumors, and another patient had two invasive lobular carcinoma tumors. *1* = invasive ductal carcinoma ($n = 5$), *2* = metastatic neuroendocrine carcinoma ($n = 1$), *3* = invasive lobular carcinoma ($n = 3$), *4* = enhancing tissue adjacent to invasive ductal carcinoma ($n = 5$), *5* = fibroadenoma ($n = 1$), *6* = benign mass ($n = 3$), *7* = areolar or nipple tissue ($n = 8$), *8* = enhancing normal tissue ($n = 7$). No more than one normal tissue ROI was derived from any given patient.

Evaluation of the clinical value of imaging modalities sensitive to breast vascularity, such as MR imaging and Doppler US (31), is also an active area of investigation. The value of temporal parameters derived from dynamic contrast-enhanced MR imaging in helping distinction of benign and malignant masses is an area of debate. Currently, there is disagreement among investigators who have performed clinical studies to evaluate the optimal method for performing contrast-enhanced MR imaging for the characterization of breast masses. As mentioned, technical factors related to volume of tissue coverage, temporal sampling rate, and quantification of temporal parameters are variable

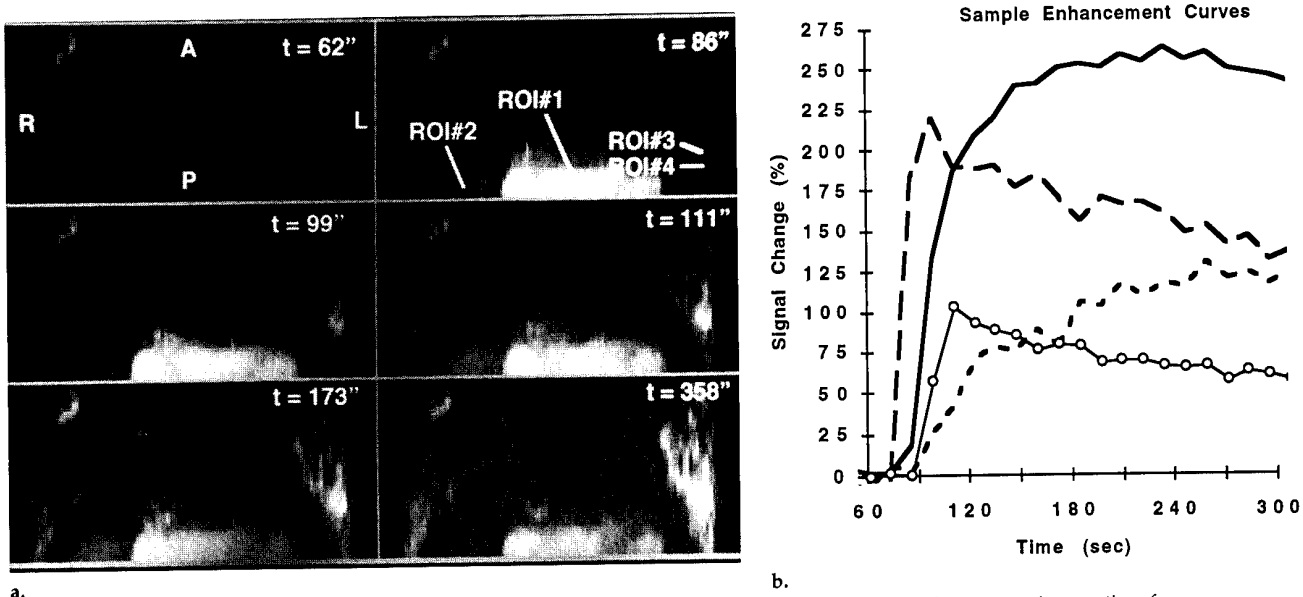


a. b.

**Figure 4.** **(a)** Maximum intensity projection of subtraction images in the superior-inferior projection. Six noncontiguous time frames are shown from images normally viewed cinegraphically. *ROI#3* delineates an invasive ductal carcinoma. Enhancement in linear structures delineates vessels. *A* = anterior, *L* = left, *P* = posterior, *R* = right, *t* = time (seconds). " = seconds. **(b)** Corresponding enhancement-time-course curves for ROIs 1–4 illustrate changes in relative rate and intensity of enhancement. Curves were derived from ROIs drawn on related single-section cinegraphic displays. *ROI#1* = left ventricular blood (broken line), *ROI#2* = liver (○), *ROI#3* = invasive ductal carcinoma (solid line), *ROI#4* = area adjacent to mass (dashed line).

across these studies. The immediate technical objectives of this study were to overcome these critical limitations. These objectives are largely met with the 3D keyhole technique, which offers full tissue coverage at high temporal sampling for subsequent quantitative enhancement time characterization. As we have discovered, the ability to dynamically study entire breasts at MR imaging, thus obviating prospective identification of one or all lesions amidst complex contrasts, is a great practical advantage. A drawback of this approach is the large data volume generated per case. Currently, we resolve the data management issue by performing reconstruction, display, and analysis on an off-line workstation with customized software tools. Our software has been specifically designed to present data in a variety of formats for specific purposes, such as the survey of all tissues in cinegraphic maximum-intensity-projection images of subtraction images or the cinegraphic viewing of a single section for quantitative analysis of individual tissues. This method also benefits from the other well-known features of breast MR imaging, such as the ability to image breasts with dense parenchyma or implants and to provide high-quality reformatted tomographic views that can potentially aid planning for surgery. ■

**Acknowledgment:** The authors thank James Pipe, PhD, for providing assistance with Advanced Visual Systems software.

## References

1. Stelling CB, Powell DE, Mattingly SS. Fibroadenomas: histopathologic and MR imaging features. Radiology 1987; 162:399–407.
2. Turner DA, Alcorn FS, Adler YT. Nuclear magnetic resonance in the diagnosis of breast cancer. Radiol Clin North Am 1988; 26:673–687.
3. el Yousef SJ, O'Connell DM, Duchesneau RH, Smith MJ, Hubay CA. Benign and malignant breast disease: magnetic resonance and radiofrequency pulse sequences. AJR 1985; 145:1–8.
4. Heywang SH, Fenzl G, Hahn D, et al. MR imaging of the breast: comparison with mammography and ultrasound. J Comput Assist Tomogr 1986; 10:615-620.
5. Heywang SH, Bassermann R, Fenzl G, et al. MRI of the breast: histopathologic correlation. Eur J Radiol 1987; 7:175-182.
6. Wiener JI, Chako AC, Merten CW, Gross S, Coffey EL, Stein HL. Breast and axillary tissue MR imaging: correlation of signal intensities and relaxation times with pathologic findings. Radiology 1986; 160:299–305.
7. Heywang SH, Hahn D, Schmidt H, et al. MR imaging of the breast using gadolinium-DTPA. J Comput Assist Tomogr 1986; 10:199–204.
8. Heywang SH, Wolf A, Pruss E, Hilbertz T, Eiermann W, Permanetter W. MR imaging of the breast with Gd-DTPA: use and limitations. Radiology 1989; 171:95–103.
9. Pierce WB, Harms SE, Flamig DP, Griffey RH, Evans WP, Hagans JE. Three-dimensional gadolinium-enhanced MR imaging of the breast: pulse sequence with fat suppression and magnetization transfer contrast—work in progress. Radiology 1991; 181:757–763.
10. Harms SE, Flamig DP, Hesley KL, et al. MR imaging of the breast with rotating delivery of excitation off resonance: clinical experience with pathologic correlation. Radiology 1993; 187:493–501.
11. Harms SE, Flamig DP. MR imaging of the breast: technical approach and clinical experience. RadioGraphics 1993; 13:905–912.
12. Heywang-Kobrunner SH. Contrast-enhanced magnetic resonance imaging of the breast. Invest Radiol 1994; 29:94–104.
13. Kaiser WA, Zeitler E. MR imaging of the breast: fast imaging sequences with and without Gd-DTPA. I. Preliminary observations. Radiology 1989; 170:681–686.
14. Stack JP, Redmond OM, Codd MB, Dervan PA, Ennis JT. Breast disease: tissue characterization with Gd-DTPA enhancement profiles. Radiology 1990; 174:491–494.
15. Hachiya J, Seki T, Okada M, Nitatori T, Korenaga T, Furuya T. MR imaging of the breast with Gd-DTPA enhancement: comparison with mammography and ultrasonography. Radiat Med 1991; 9:232–240.
16. Kaiser WA. MR mammography. Radiologe 1993; 33:292–299.
17. Orel SG, Schnall MD, Li Volsi VA, Troupin RH. Suspicious breast lesions: MR imaging with radiologic-pathologic correlation. Radiology 1994; 190:485–493.
18. Schnall MD, Orel S, Muenz L. Analysis of time intensity curves for enhancing breast lesions (abstr). In: Proceedings of the Society of Magnetic Resonance in Medicine 1993. Berkeley, Calif: Society of Magnetic Resonance in Medicine, 1993; 120.
19. Harms SE, Flamig DP, Hesley KL, et al. Fat-suppressed three-dimensional MR imaging of the breast. RadioGraphics 1993; 13:247–267.
20. van Vaals JJ, Brummer ME, Dixon WT, et al. "Keyhole" method for accelerating imaging of contrast agent uptake. J Magn Reson Imaging 1993; 3:671–675.
21. Chenevert TL, Pipe JG. Dynamic 3D imaging at high temporal resolution via reduced k-space sampling (abstr). In: Proceedings of the Society of Magnetic Resonance in Medicine. Berkeley, Calif: Society of Magnetic Resonance in Medicine, 1993; 1262.
22. Spraggins TA, de Paredes ES, De Angelis GA, Thiele F. Three keyhole imaging: ap-

plication to dynamic contrast enhanced MRI of breast lesions (abstr). In: Proceedings of the Society of Magnetic Resonance in Medicine. Berkeley, Calif: Society of Magnetic Resonance in Medicine, 1993; 118.
23. Press WH, Flannery BP, Teukolsky SA, Vetterling WT. Numerical recipes. Cambridge, Mass: Cambridge University Press, 1989; 523–528.
24. Hennig J, Nauerth A, Friedburg H. RARE imaging: a fast imaging method for clinical MR. Magn Reson Med 1986; 3:823–833.
25. Mulkern RV, Melki PS, Jakob P, Higuchi N, Jolesz FA. Phaseencode order and its effect on contrast and artifact in singleshot RARE sequences. Med Phys 1991; 18:1032–1037.
26. Harris AL, Horak E. Growth factors and angiogenesis in breast cancer. Recent results. Cancer Res 1993; 127:35–41.
27. Weidner N, Semple JP, Welch WR, Folkman J. Tumor angiogenesis and metastasis: correlation in invasive breast carcinoma. N Engl J Med 1991; 324:1–8.
28. Horak ER, Leek R, Klenk N. Angiogenesis, assessed by platelet/endothelial cell adhesion molecule antibodies, as indicator of node metastases and survival in breast cancer. Lancet 1992; 340:1120–1124.
29. Folkman J. What is the evidence that tumors are angiogenesis dependent (editorial)? J Natl Cancer Inst 1990; 82:4–6.
30. Jensen HM, Chen I, De Vault MR, Lewis AE. Angiogenesis induced by "normal" human breast tissue: a probable marker for precancer. Science 1982; 218:293–295.
31. Cosgrove DO, Kedar RP, Bamber JC, et al. Breast diseases: color Doppler US in differential diagnosis. Radiology 1993; 189:99–104.